Self-Assembly of Chiral Nanoparticle Pyramids with Strong *R/S* Optical Activity

Wenjing Yan,[†,#] Liguang Xu,[†,#] Chuanlai Xu,[†,#] Wei Ma,[†,§,#] Hua Kuang,*[,†] Libing Wang,*[,†,‡] and Nicholas A. Kotov*[,§]

[†]School of Food Science and Technology, State Key Lab of Food Science and Technology, Jiangnan University, Wuxi, JiangSu 214122, People's Republic China

[‡]Technological Center of Hunan Entry-Exit Inspection and Quarantine Bureau, Changsha 410001, People's Republic China

[§]Department of Chemical Engineering, University of Michigan, Ann Arbor, Michigan 48109, United States

S *Supporting Information*

ABSTRACT: Chirality at the nanometer scale represents one of the most rapidly developing areas of research. Self-assembly of DNA−nanoparticle (NP) hybrids enables geometrically precise assembly of chiral isomers. The concept of a discrete chiral nanostructure of tetrahedral shape and topology fabricated from four different NPs located in the corners of the pyramid is fundamental to the field. While the first observations of optical activity of mixed pyramidal assemblies were made in 2009 (Chen, W.; et al. *Nano Lett.* **2009**, 9, 2153−2159), further studies are difficult without finely resolved optical data for precisely organized NP pyramidal enantiomers. Here we describe the preparation of a family of self-assembled chiral pyramids made from multiple metal and/or semiconductor NPs with a yield as high as 80%. Purposefully made *R*- and *S*-enantiomers of chiral pyramids with four different NPs from three different materials displayed strong chiroptical activity, with anisotropy *g*-factors as high as 1.9×10^{-2} in the visible spectral range. Importantly, all NP constituents contribute to the chiroptical activity of the *R/S* pyramids. We were able to observe three different circular dichroism signals in the range of 350−550 nm simultaneously. They correspond to the plasmonic oscillations of gold, silver, and bandgap transitions of quantum dots. Tunability of chiroptical bands related to these transitions is essential from fundamental and practical points of view. The predictability of optical properties of pyramids, the simplicity of their self-assembly in comparison with lithography, and the possibility for polymerase chain reaction-based automation of their synthesis are expected to facilitate their future applications.
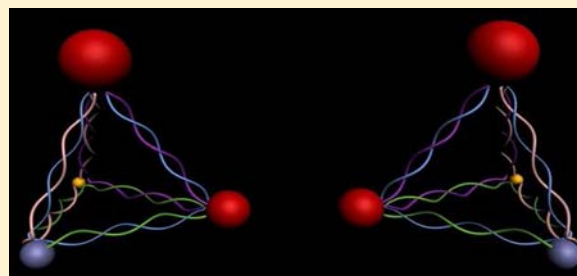
INTRODUCTION

Chirality determines many structure−function relationships in Nature[1,2] at many levels of biological organization. Such omnipresence of chiral properties in biology inspires and necessitates further studies of chirality of nanoscale materials due to many structural parallels between nano- and biomaterials as well as multiple biomedical applications of nanoparticles (NPs). Despite some important advances in this area discussed below, we are still far from their systematic understanding and utilization. The technologies where chiral nanomaterials could find direct applications span the range from drug delivery to optical devices utilizing negative refraction phenomena.

Chirality of biological objects can be traced to the tetrahedral geometry of sp³-hybridized carbon with four different substituents. While similar origin of chirality is possible for NPs,[3] dominant mechanisms by which the nanostructures can acquire chiral properties are, so far, different. Organic molecules with chiral orbitals can become hybridized and thereby "share" this property with non-chiral electronic states on the NP surface.[4,5] Such mechanism can be traced for many inorganic NPs,[3,6−15] nanotubes,[16,17] and nanorods (NRs).[18,19] Imprinting

chiral electronic structure of organic molecules on inorganic NPs can be particularly strong for plasmonic nanostructures as compared to semiconductor ones. Their chirality can manifest as strong optical activity in the plasmonic region and as enhancement of the intrinsic chirality of organic molecules localized in plasmonic gaps. At the same time, intrinsically chiral nanostructures regardless should give much stronger optical activity, as could be seen from the original findings in chiral assemblies[21] and a very recent publication on this subject regarding individual NPs.[20] Plasmonic NPs were also the subject of the early papers on configurational chirality at the nanoscale related to the geometrical disposition of non-chiral NPs,[21,22] which was later extended to helical arrangements of NRs[10] and NPs,[23−25] and tetrahedral arrangements of nanoscale disks.[26] Compared with chirality from individual NPs, the collective chirality generated from NP assemblies is likely to give significantly higher anisotropy coefficients, *g*, in the visible range, as was suggested by both experimental[26] and theoretical

ACS Publications © 2012 American Chemical Society

15114

dx.doi.org/10.1021/ja3066336 | *J. Am. Chem. Soc.* 2012, 134, 15114−15121

studies.[4] Chiral plasmonic systems are of interest for negative index materials[27,28] and sensors[29] among other potential applications.

Pairing of DNA oligomers represents a convenient tool for creation of NP assemblies,[23−25,30,31] leading to both discrete and extended systems.[32] Selective DNA hybridization enables geometrically precise assembly of chiral isomers. Interestingly, this ability is probably theoretically appreciated but practically under-utilized. There are only a few studies on chiral superstructures using DNA linkers, focusing on two fundamental structures possessing chirality, tetrahedrons and helices.[20,21,23,24,32] Although making chiral tetrahedral systems initiated the field in 2009,[21,22] making helical structures has received more attention recently, possibly due to simpler preparative methods. Experimental observations of helical NP superstructures can possibly be exemplified by twisted ribbons described by Srivastava et al.[23a] and then Lilly et al.;[23b] however, these systems failed to demonstrate any enantiomeric preference in the mixtures of left and right NP helices. Recently Kuzyk et al.[24] and Shen et al.[25] prepared chiral assemblies of gold nanoparticle (AuNP) helices for which a clear chiral response was observed due to application of DNA origami technique.

The concept of a discrete chiral nanostructure of tetrahedral shape fabricated from four different NPs located in the corners of the pyramid is very fundamental to the field. Making pyramids from four NPs connected by DNA was attempted in the past.[21,22] Mastroianni et al.[22] discussed preparation of chiral tetrahedrons from AuNPs with different sizes, but no data on chiroptical properties of such DNA-based NP assemblies were reported. At the same time, Chen et al.[21] measured polarization rotation originating from several chiral structures present in the optical media, but did not identify the actual enantiomers responsible for the observed chiral plasmonic peaks. Fan et al.[33] theoretically described the fact that helices and tetrahedrons of plasmonic particles should have optical activity using electrodynamic formalism. Their paper was focused on an approach to simulate circular dichroism (CD) spectra and confirmed the appearance of a CD band at the position of gold plasmons previously observed by Chen et al.[21]

Importantly, *the actual optical activity of systematically made NP pyramids has never yet been observed.* The same is true for the preparation of pyramids from spatially organized NPs from different materials, such as metals and semiconductors, because they produce optical activity in different parts of the optical spectrum. The importance of practical implementation of chiral pyramids made from DNA-modified NPs arises from (1) their geometrical simplicity and predictability of this structure, amenable to theoretical evaluation by different methods; (2) the self-assembly mechanism of their formation, which is much easier than lithography;[26] and (3) the exciting possibility to use standard polymerase chain reaction techniques to scale-up and automate their synthesis for practical applications of chiral materials.[21,34]

In this work, we describe the preparation and optical properties of a variety of NP pyramids made by DNA-driven self-organization from individual building blocks. They comprise small AuNPs (10 nm, Au_1), medium AuNPs (15 nm, Au_2), large AuNPs (25 nm, Au_3), CdSe@ZnS quantum dots (5 nm, QDs), and silver NPs (10 nm, Ag). Besides achieving the fundamental milestones for the studies of chiral properties at nanoscale, we observed high optical activity with g-factors significantly exceeding those of traditional optically active materials. It is also significant to point out that the synthetic yield of these pyramids is approaching 80%, which opens extensive opportunities for further research and instills stronger confidence in the viability of chirality-based optical devices.

■ EXPERIMENTAL SECTION

Materials. Thiolated DNA oligonucleotides purified by polyacrylamide gel electrophoresis (PAGE) were purchased from Shanghai Sangon Biological Engineering Technology & Services Co. Ltd. (Shanghai, P.R. China) and suspended in deionized (DI) water to a final concentration of 100 μM. The DNA sequences are shown in the Supporting Information, Table S1. Unless stated otherwise, all chemicals used in this work were purchased from Sigma-Aldrich. DI water from a Milli-Q device (18.2 MΩ, Millipore, Molsheim, France) was used throughout this work. All glassware was cleaned with freshly prepared aqua regia and rinsed thoroughly by DI H$_2$O prior to use.

Instruments. Transmission electron microscopy (TEM) images were obtained using a JEOL JEM-2100 transmission electron microscope operating at an acceleration voltage of 200 kV. Before TEM examination, 15 μL of eacn sample was dried in air, dispersed onto a copper grid coated with the carbon film. The 3D spatial arrangement of NP assemblies was characterized by an FEI Titan Krios instrument equipped with a Gatan UltraScan 4000 (model 895) 16-megapixel CCD, the instrument operated at an accelerating voltage of 300 kV. The samples were prepared on the surface of copper net. The chirality of nanostructures was characterized by MOS-450/AF circular dichroism. The sizes of NPs and assemblies were achieved using dynamic light scattering (DLS; Malvern Zetasizer Nano-ZS, 633 nm laser). All UV/vis results were acquired on a UNICO 2100 PC UV/vis spectrophotometer and processed with the Origin Lab software. Synchrotron small-angle X-ray scattering (S-SAXS) experiments were carried out at room temperature at the BL16B1 beamline at the Shanghai Synchrotron Radiation Facility, Shanghai Institute of Applied Physics, China, operated at 3.5 GeV with injection currents of 300 mA. The scattering data were collected with a MAR CCD area detector at wavelength λ = 1.5498 Å.

Synthesis of Gold Nanoparticles. Three different sizes of AuNPs were used in this work. AuNPs with diameters of 10 ± 2 nm (Au_1), 15 nm ± 2 nm (Au_2), and 25 ± 3 nm (Au_3) were synthesized according to the previous methods.[35,36] Typically, all glassware were soaked with aqua regia (volume ratio 3:1, HCl/HNO$_3$) and washed thoroughly with Millipore-Q water several times. Bigger NPs (15 ± 2 or 25 ± 3 nm) were fabricated by reduction of HAuCl$_4$ using trisodium citrate.[35] Briefly, aqueous trisodium citrate solution (2.0 or 1.6 mL, 1% by weight, freshly prepared) was quickly added to a boiling aqueous solution of HAuCl$_4$ (100 mL, 0.25 mM) under vigorous stirring and reflux. Several minutes later, the color of the solution changed from blue to wine red. After 15−30 min of boiling, the heat source was removed to allow the reaction solution to cool to room temperature. Small NPs (10 ± 2 nm) were synthesized by sodium citrate−tannin reduction.[36] First, 1 mL of HAuCl$_4$ (1% by weight) was added into 79 mL of Millipore-Q water under stirring; the mixture was prepared as solution A. Second, 4 mL of sodium citrate (1% by weight), 0.1 mL of tannic acid (1% by weight), and 0.1 mL of K$_2$CO$_3$ (25 mM) were added into 15.8 mL of Millipore-Q water; the sample was mixed under stirring and named as solution B. Third, solutions A and B were respectively heated to 60 °C for 30 min, and then solution B was quickly added into solution A under high-speed stirring. The solution was kept at 60 °C for 30 min until the color turned to reddish orange and did not change, and then cooled to room temperature. The dimensions of the NPs were characterized by TEM, and the solutions were subsequently stored at 4 °C.

In order to make sure the AuNPs modified with less DNA were well-dispersed at high ionic strength, phosphine ligand [bis(p-sulfonatophenyl)phenylphosphine dihydrate, dipotassium salt (BPS)] was used to protect AuNPs followed modified Loweth's method.[37] Aqueous solutions (10 mL) of 10 ± 2, 15 ± 2, and 25 ± 3 nm AuNPs at initial concentrations of 10, 8, and 2 nM were stirred with excess

15115

dx.doi.org/10.1021/ja3066336 | J. Am. Chem. Soc. 2012, 134, 15114−15121

BPS (40, 20, and 10 mg/mL) at room temperature for 10 h. The solutions were then centrifuged at different speeds (13000, 10000, and 7000 rpm). The supernatants were removed, and the resulting pellets were resuspended in water.

Synthesis of Silver Nanoparticles. AgNPs with a diameter of 10 ± 3 nm were synthesized following the previously described method with some modifications.[38,39] Briefly, 0.6 g of NaBH$_4$ was dissolved in 20 mL of distilled water (ice-cold), and then 5 mL of 1% poly(vinyl pyrrolidone) (PVP) was added as stabilizer (protecting agent). The solution was kept in a water−ice bath with high-speed stirring. Next, 5 mL of 1% PVP and 5 mL of 10 mM AgNO$_3$ were added to the mixture prepared beforehand simultaneously by two constant-flow pumps at the rate of 30 mL/h. The solution was kept at 80 °C for 3 h to remove the unreacted NaBH$_4$; the prepared sample was yellow and was stored at 4 °C.

Preparation of Single-Strand DNA-Modified AuNPs. Classical citrate-protected AuNPs (Au$_1$, Au$_2$, Au$_3$) prepared beforehand were functionalized with 87-base thiolated ssDNA according to the reported method.[40] In order to avoid the formation of plasmonic polymer and simultaneously improve DNA coupling efficiency to the surface of AuNPs, BPS-protected AuNPs were mixed with ssDNA in a ratio of 1:1 and incubated for 2 h in 0.5×TBE, 50 mM NaCl. The samples were then centrifuged at 13000, 10000, or 7000 rpm for 10 min to remove uncoupled oligonucleotides from solution. The supernatants were removed, and the pellet was resuspended in water.

For the purpose of improving the yield of the reaction, density gradient centrifugation was used to separate AuNPs and DNA−AuNP conjugates.[41] Briefly, a step gradient was created directly in an Eppendorf tube (polystyrene, 1.5 mL) to make a 15% + 60% gradient (15% + 40% was used to separate small NPs−DNA conjugate). Briefly, 500 μL of 15% Ficoll400 solution was added to the centrifuge tube first, and then 500 μL of 60% (40%) Ficoll400 solution was carefully added below the 15% layer by inserting a pipet to the bottom of the centrifuge tube. The purified Au−DNA conjugate was then carefully layered on top of the density gradient. The sample was centrifuged at 5000 rpm for 40 min. The supernatants were removed, and the pellet was re-suspended in water. After centrifugation two times, high-yield Au−DNA conjugates were obtained.

Fabrication of Single-Strand DNA-Modified AgNPs. PVP with a long chain of C−H group prevented the reunion between silver ions and increased the stability of AgNPs in highly ionic solution. AgNPs and SH-DNA were incubated overnight in a ratio of 1:4 in 0.5×TBE buffer, 50 mM NaCl. The sample was then centrifuged at 13000 rpm for 10 min. The supernatant was removed, and the pellet was resuspended in water. DNA−AgNP conjugate was purified using the same method as for AuNPs.

Preparation of Single-Strand DNA-Modified Quantum Dots. CdSe@ZnS core/shell quantum dots (QDs) carrying carboxyl-COOH surface ligands were purchased from Wuhan Jiayuan Quantum Dots Co., Ltd. (Wuhan, China). QDs were functionalized with amino-modified ssDNA by using carbodiimide chemistry.[42] 1-(3-Dimethyla-minopropyl)-3-ethylcarbodiimide hydrochloride (EDC) and N-hydroxysuccinimide (NHS) were used as zero-length cross-linkers. The conjugation protocol is simple and takes approximately 4 h. Briefly, QD, EDC, and NHS at a molar ratio of 1:1000:200 were reacted for 10−15 min in the dark at room temperature. Amino-modified DNA was then added to the sample in a 1:5 ratio, and the solution was incubated for 3 h with shaking in the dark at room temperature. QD−ssDNA conjugates were purified by ultrafiltration (30k molecular weight cutoff) to remove the non-conjugated ssDNA.[43] QDs with emission wavelength of 608 nm were used.

Self-Assembly of Chiral Pyramids. In this work, a two-step method was used to prepare chiral pyramids of different types. First, homogeneous or heterogeneous pairs were formed by mixing two identical or different NP−DNA conjugates bearing partially complementary ssDNA in 0.5×TBE buffer, 50 mM NaCl. The hybridization mixtures were heated at 90 °C for 5 min and then slowly cooled to room temperature.[44,45] High temperatures made long-chain DNA denatured to an open end and improved the hybridization of DNA to expected structures in the process of temperature reduction. These well-assembled dimer structures provide a good condition for the configuration of chiral pyramids. Two symmetric or asymmetric pairs were mixed in 1×TBE buffer, 50 mM NaCl; the sample was stirred for 24 h at room temperature to give the desired pyramids.

■ RESULTS AND DISCUSSION

Structural Design and Assembly. In this work, plasmonic NPs and/or semiconductor NPs modified with four different single-strand DNA (ssDNA) as building blocks were purposefully selected to gain geometrical precision of their assembly (Scheme 1). Four ssDNA sequences (see Table S1)

Scheme 1. Synthesis of Chiral NP Pyramid
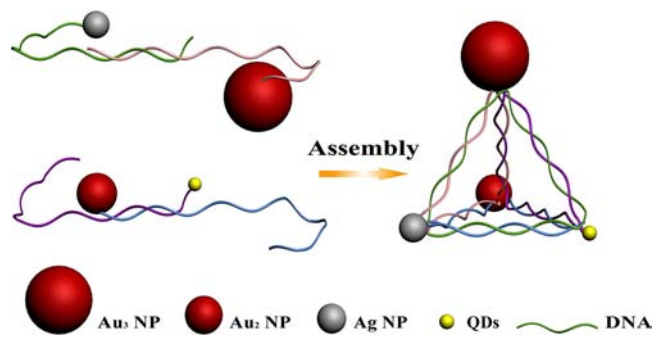
can complementarily hybridize with each other. Each of them can be segmented into three pieces. Each piece is complementary to a third of each of the other strands. So, each strand of DNA "weaves" through three pyramid sides outlining one face of the pyramid with a perimeter length of 26 bp. Three thymine bases were inserted in the corners forming the kink points between the segments in order to add sufficient flexibility to the DNA without straining the structure. This aspect of structural design is significant for the successful preparation of tetrahedral superstructures. Four NPs acted as the connecting vertices located in the apexes of the tetrahedron. It might be useful to highlight the fact that with this approach the assemblies are made as specific enantiomers: Just like one can construct mirror images of tetrahedra from macroscale educational kits on molecules, the same can be done at nanoscale with DNA oligomers. In many other cases of chiral structures including tetrahedral orientations of atoms in apexes of NPs with zinc blend crystal lattice,[3] the chiroptical properties are achieved by increasing the concentration of one enantiomer over another. This constitutes breaking of chiral equivalence using a slight thermodynamic or kinetic preference of one enantiomer over another.

Preparation of Dimers and Structural Characterization. To gain the necessary structural control over the placement of the NPs, we employed a two-step assembly process with dimers as intermediates, which also greatly improved the yield of the pyramids and, consequently, the accuracy of the elucidation of their chiral properties. NP dimers were prepared as the first stage of the synthesis by hybridizing two complementary NP−DNA conjugates at 90 °C for 5 min. NP−DNA conjugates were prepared by a protocol reported previously with modifications[40−43] which allows one also control the amount of ssDNA attached to the surface of NPs and, therefore, the yield and precision of the assemblies. Figure 1A−E shows representative TEM images of five types of NP dimers. Statistical analysis of as many as 200 images for each construct indicated that the yields for the intended NP pairs
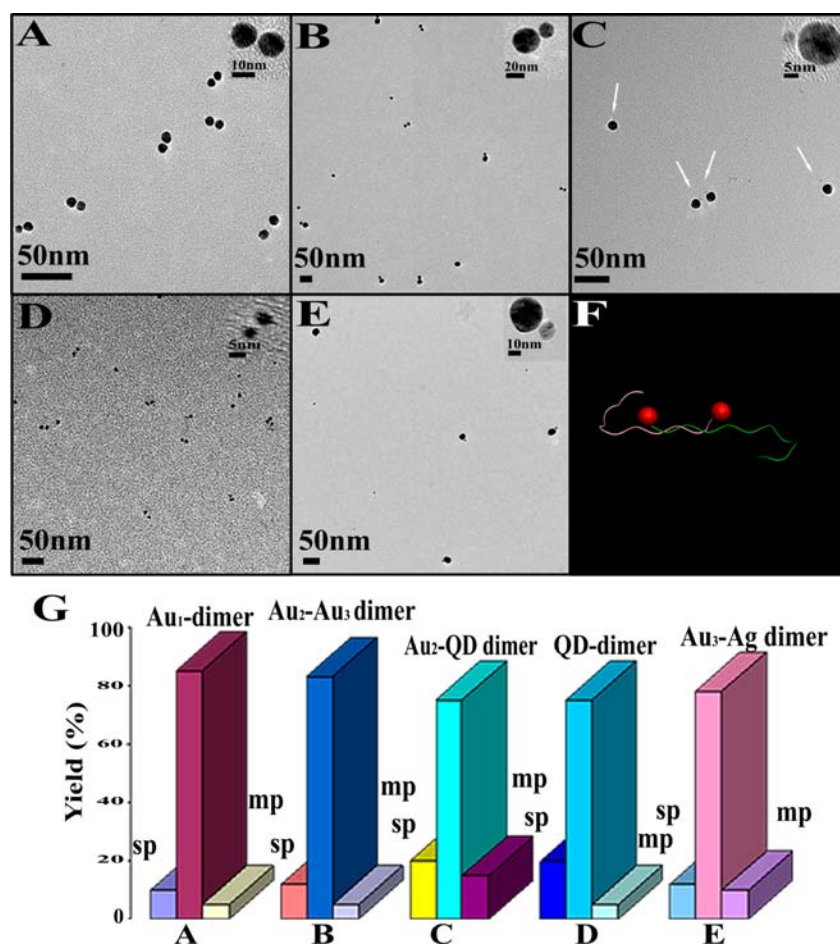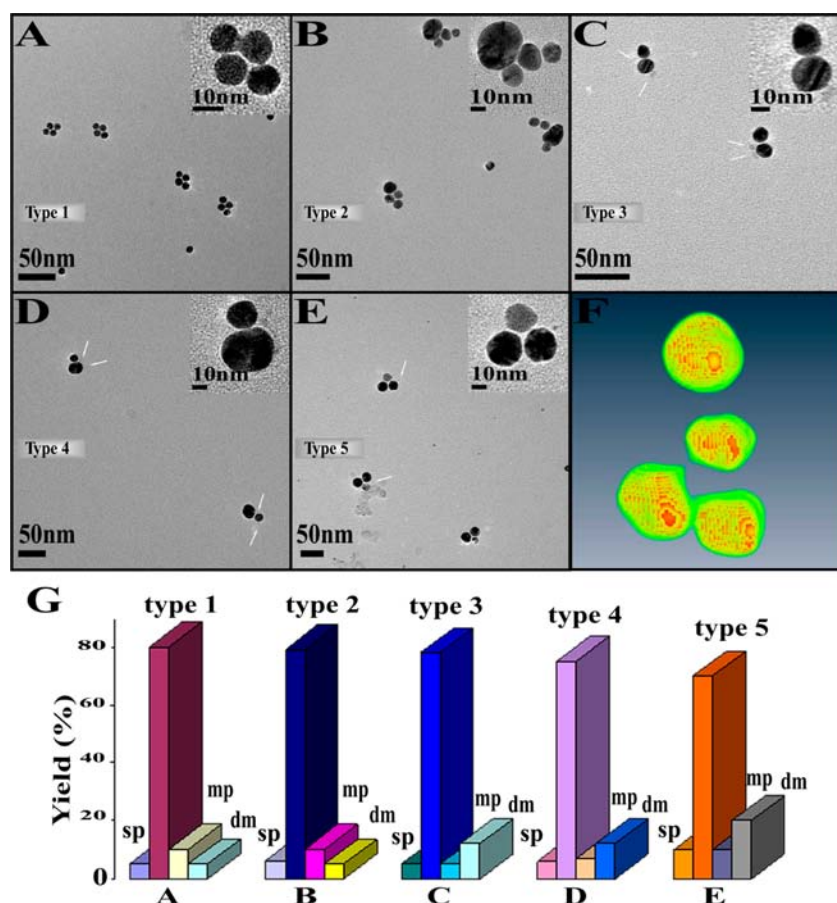
Figure 1. (A−E) Representative TEM images of (A) Au_1 dimer, (B) Au_2−Au_3 dimer, (C) Au_2−QD dimer (QDs are marked with white arrows), (D) QD dimer, and (E) Au_3−Ag dimer. (F) Schematics of synthetic method for plasmonic dimer using DNA hybridization. (G) Statistical analysis of different products in the reactions of dimer assembly in A−E. Notations "sp" and "mp" stand for single-particle and multiparticle assemblies (>2), respectively.

were as high as 75−85% (Figure 1G). Agarose gel electrophoresis data (Figures S2 and S3) unambiguously confirmed the formation of NP dimers[46] and indicated that heavier constructs make only minor contribution to the assembly products. Optical spectroscopy data further affirmed the formation of the dimers with projected combinations of NPs (Figure S4). All of the dimers displayed small red-shifts of UV−vis absorption bands with respect to those of monomers or unconjugated mixtures of NPs. The red-shift is consistent with plasmonic effects in NP pairs positioned in proximity to each other. Emission of semiconductor NPs is strongly quenched in the heteroparticle dimers by metallic NPs (Figure S5), as expected from the previous studies.[47] Note that the maximum distance between two NPs in the dimers is determined by the 26 bp double-strand DNA (dsDNA) bridge equal to 8.8 nm, which agrees very well with the radius of QD fluorescence quenching by metal NPs.[48]

The combination of S-SAXS and DLS data gave us strong evidence for the actual space occupied by the NPs and their assemblies in a "wet" state rather than in the "dry" state characteristic for TEM. This is significant in order to understand better the degree of expansion upon hydration as well as the ensemble composition of the dispersion. S-SAXS could be particularly informative because one could obtain information about different nanoscale superstructures in terms of size, shape, and conformation by looking at S-SAXS features

located at different scattering vectors.[49−52] In the small scattering vector q region ($q < 0.01$ Å^{-1}), distinct scattering patterns were observed for the NP assemblies (Figure S6A). The peak at $q = 0.00469$ Å^{-1} can be attributed to Au_1 dimer. S-SAXS of the dimer shows 21 ± 0.5 nm to be its longest measure. Although this average size corresponds very well to the dimer dimensions seen in TEM images, the actual gap between Au_1 NPs with diameter 10 nm is likely to be underestimated due to their elongated shape and S-SAXS corrections needed in this case. Importantly, S-SAXS data also indicate that there is no substantial amount of heavier agglomerates present in the dispersion, since this technique is very sensitive to the species with large scattering profile expected to strongly shift the observed peak.

DLS is a well-established technique for measuring the size and size distribution of particles and molecules in liquids.[51] The ensemble-averaged diameter of the dimers can also be characterized by DLS, although size estimations lower in accuracy than those obtained with S-SAXS could be expected. The DLS diameter of a Au_1 dimer was measured to be 26 ± 3 nm, which is slightly larger than the dimensions obtained by S-SAXS and TEM. The gap between two Au_1 NPs (10 nm) can be estimated to be 9 nm, which is most likely an upper limit of the potential gap length (Figure S6B). Similarly to S-SAXS and TEM, we see virtually no DLS signal corresponding to particles with hydrodynamic dimensions above 60 nm. From this

Figure 2. Representative TEM images of self-assembled pyramids made from (A) four Au_1 (type 1), (B) three Au_2 + Au_3 (type 2), (C) two Au_2 NPs + two QDs (type 3), (D) Au_2 + Au_3 + two QDs (type 4), and (E) S-enantiomer Au_2 + Au_3 + Ag + QD (type 5). (F) Typical TEM tomography image of the four Au_1 pyramid (type 1). (G) Statistical analysis of different products in the reactions of pyramid assembly given in A−E. Notations "sp", "dm", and "mp" stand for single-particle, dimers, and multiparticle assemblies (>2), respectively. The QDs in C−E are marked with white arrows.

observation one should infer that there could be some dimers and trimers, but it is unlikely that there are any heavier aggregates present. Importantly, there are no peaks corresponding to either of them, indicating the dominance of dimers in accordance with Figure 1G.

Preparation of Chiral Pyramids with Tunable Chiroptical Responses. Two selected NP dimers were hybridized together to assemble pyramids of required geometry. Six different types of pyramids were made with variable geometrical placement, size, and material of the NPs: all four 10 nm Au_1 (type 1), three 15 nm Au_2 + 25 nm Au_3 (type 2), two Au_2 + two QDs (type 3), Au_2 + Au_3 + two QDs (type 4), and S- (type 5) and R-enantiomers (type 6) of Au_2 + Au_3 + QD + Ag. The TEM images of these pyramids at different magnifications are given in Figure 2A−E; schematics of their geometries are given in Figure 3. The dispositions of all NPs in typical TEM images match two-dimensional projections of pyramids in Figure 3 very well. TEM tomography and three-dimensional images of pyramids (Figure 2F) indicate approximately tetrahedral geometry, although somewhat distorted, possibly by drying. S-SAXS and DLS dimensions of the pyramid did not change appreciably compared to the dimer (Figure S6) as expected.

A special note needs to be made about R/S designations of pyramidal enantiomers made from NPs. It is based on the extension of the Cahn−Ingold−Prelog priority (CIP) rule used in organic chemistry. We consider that the chiral center is located in the geometrical center of the pyramid. As in classical CIP rule, the priority is assigned based on the atomic number (Z) of the heaviest atom in the core of NPs/QDs. If the heaviest atom is the same (as in Au_1, Au_2, and Au_3), higher priority is assigned to NPs with larger diameters. For the specific case of pyramids described here, the priority of NPs is, therefore, Au_3 > Au_2 > Au_1 (Z_A = 79) > QD (Z_{Cd} = 48) > Ag (Z_{Ag} = 47). The yield of the dimer-to-pyramid assembly step was as high as 80% (Figure 2G), which matched the data obtained in other DNA-driven assemblies of discrete NP−NR superstructures.[51] Since we can assemble the specific enantiomer by design not relying on breaking chiral equivalence and with such high yield, the R/S designators could be assigned based on the expected structure. Assigning the chirality of the clusters using TEM tomography (Figure 2F) is also possible since this method can potentially pinpoint the location of each NP in 3D space very well.

Chiroptical Properties. The high yield of NP assemblies allowed us to perform a detailed characterization of their optical activity. Compared with the little changes in the UV−vis spectra (Figure S7), the chiroptical activity of the pyramid becomes more pronounced. We started with the evaluation of chiroptical activity of individual building blocks, i.e., ssDNA, AuNPs, QDs, and AgNPs and discrete nanocrystal/DNA conjugates (Au−DNA, Ag−DNA, and QD−DNA). Part of them displayed expected CD activity in 200−300 nm region,
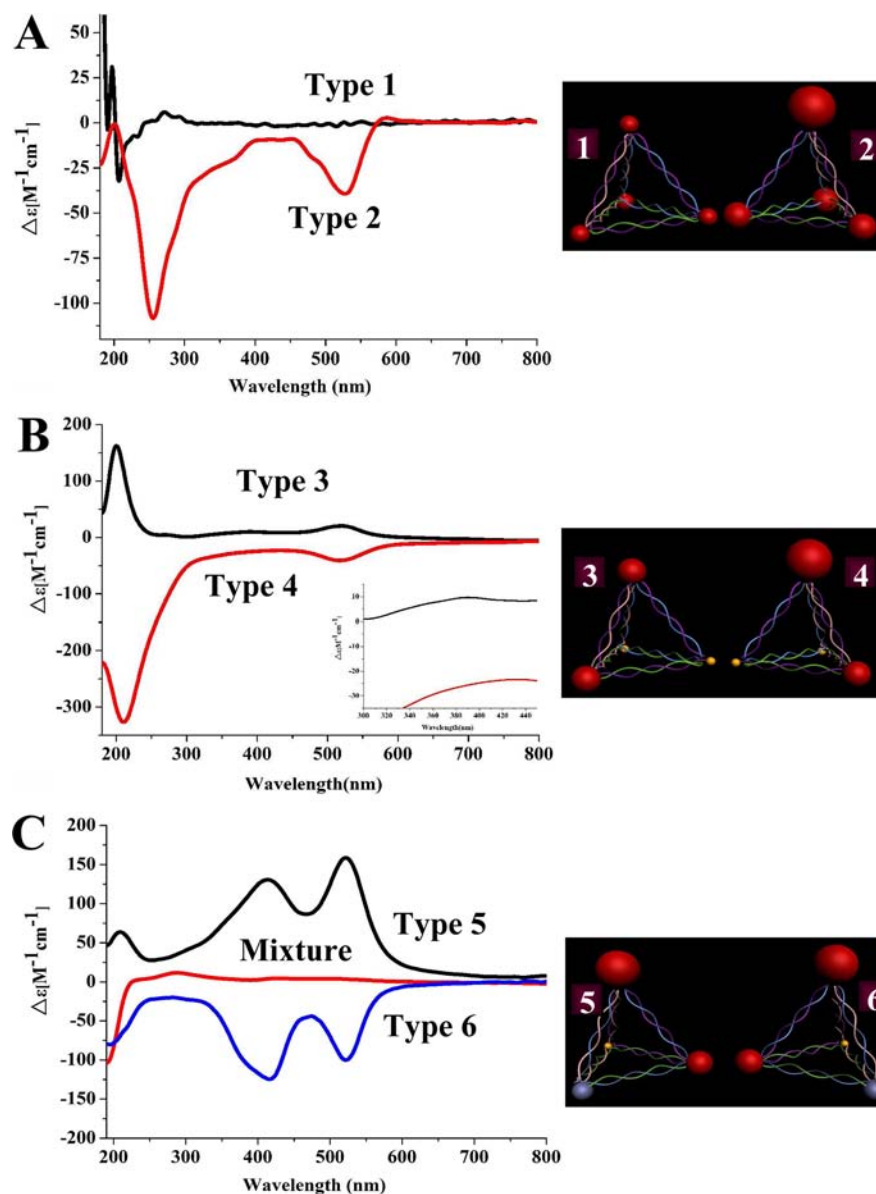
Figure 3. Circular dichroism spectra of self-assembled pyramids made from (A) four Au_1 (type 1) and three Au_2 + Au_3 (type 2); (B) two Au_2 + two QDs (type 3), and Au_2 + Au_3 + two QDs (type 4) [inset: CD spectrum in 300–450 nm region]; and (C) Au_2 + Au_3 + Ag + QD as S- (type 5) and R-enantiomers (type 6).

but no CD peaks for the spectral range from 350 to 550 nm (Figure S8) associated with optical transitions in QDs and NPs used here. The CD bands in the 200–300 nm region should be assigned to DNA oligomers which typically display chiral signal at these wavelengths. One should not exclude the possibility that other CD bands, for instance those associated with chiral centers on a NP surface,[3] can appear in this region, too.

Type 1 pyramids displayed CD peak only in the UV-absorption region, but no chiroptical activity was detected in the spectral range of Au plasmons (Figure 3A). In this case, the symmetric pyramidal frame constructed from all-identical NPs showed no chirality at the visible range as might be expected.[53] Notably, type 2, type 3, and type 4 assemblies displayed strong CD signals in the 520–540 nm plasmonic region while not being obviously chiral. This effect could potentially be attributed to the chiral placement of NPs in space predetermined by the chiral twisting of the DNA connectors and tangible geometrical inequality of seemingly identical NPs.

As such, three-dimensional images of AuNPs in Figure 2F revealed that their shape is often not quite spherical as was often presumed before (Figure S1). Addition of one (type 2), two (type 3), or three (type 4) NPs dissimilar in size (type 2) or material (types 3, 4) is sufficient to breaking the symmetric frame and amplify these subtle differences manifesting in the chiroptical activity of the resulting pyramids. Taking into account the irregular spherical shape of NPs, Coulomb and electromagnetic interactions between nanocrystals in such complexes become very prominent and govern their optical responses. Accordingly, one can see the gradual enhancement of the CD peak in plasmonic region in the order type 3 < type 2 < type 4. The plasmonic NPs play an important role in the enhancement of CD. However, the reason(s) why there is greater abundance of a specific enantiomer still needs to be understood. The preference in R- or S-enantiomer could be related to the preferential binding of DNA to geometrically specific sites on NP surfaces. Even more importantly, the

inclusion of QDs to the pyramid produces an additional weaker peak around 390 nm (inset in Figure 3B). This peak corresponds to the chiroptical activity of the bandgap transition of QDs, which was quite difficult to obtain before.[8]

We also made pyramids that contained all four different NPs. These pyramids were made of Au_2, Au_3, AgNPs, and QDs. Based on the classical CIP priority rule (see above), ($Au_3 > Au_2 > Au_1$ ($Z_A = 79$) > QD ($Z_{Cd} = 48$) > Ag ($Z_{Ag} = 47$)), the constructed NP assemblies can be labeled as *R*- or *S*-enantiomers (Figure 3C). They displayed much enhanced chiroptical activity in the visible part of the spectrum, namely between 340 and 630 nm. In addition to much enhanced CD peak corresponding to gold plasmon at 522 nm, there is also a distinct shoulder at 350 nm corresponding to the bandgap of QDs which can be seen in types 3, 4, and 5. Also we saw emergence of another strong CD peak at 410 nm which should be attributed to the plasmon of AgNPs.[11,54]

It was important to verify that the *R*- and *S*-enantiomers of chiral pyramids have opposite directions of polarization rotation. This would substantiate the essential hypothesis that chiroptical activity in discrete NP assemblies originates from geometrical disposition of NPs, and therefore, can be controlled by the assembly route. Indeed, type 5 and type 6 assemblies showed nearly perfectly opposite CD spectra in terms of the peak position and their intensity. To verify the results, we also mixed pre-made *R*- and *S*-Au_2 + Au_3 + Ag + QD pyramids in equal proportions and featureless flat line in CD spectrum was obtained (Figure 3C, red line). Importantly, the assembly of the chiral pyramids was reversible. As one can expect from the properties of DNA and as we described in our previous work,[21] NP assemblies held by DNA are sensitive to temperature and are destroyed as DNA "melts". DNA-linked nanostructures were indeed destroyed as evidenced by the shifts in UV−vis spectrum and disappearance of the CD peaks. However, upon cooling complementary ssDNA rehybridized and the super-structure reassembled. Restored CD signals of the assemblies were not affected when the DNA scaffold re-assembly process.

The intensity of optical activity of chiral pyramids was quantified using the spectral maximum, g_{max}, of the standard anisotropy *g*-factor (Figure S9).[55] Expectedly, type 1 pyramids displayed the lowest anisotropy factors with $g_{max} = 2 \times 10^{-3}$ for 517 nm among all the tetrahedral superstructures we made. Curiously, these *g*-factors are still fairly high compared to typical *g*-values seen in organic chemistry (Supporting Information). Types 2, 3, and 4 displayed $g_{max} = 6.8 \times 10^{-3}$ at 528 nm, 3.9×10^{-3} at 519 nm, and 8.1×10^{-3} at 510 nm, respectively. The increase in maximum *g*-values upon introduction of multiple NPs in the pyramid is apparent in this sequence and confirms with simple geometrical consid-erations. Type 5 and type 6 pyramids composed of Au_2, Au_3, Ag, and QD displayed the highest g_{max}, with values as high as 1.9×10^{-2} at 520 nm and 1.7×10^{-2} at 422 nm, respectively, which is much higher than those of chiral metal clusters or NPs.[56] This can be attributed to the high degree of the asymmetric geometry and the enhancement of the optical response of AgNP with larger surface plasmon resonances.[57,58] Also important is the fact that, the *g*-values corresponding to DNA at the wavelengths of 257 nm obtained in type 2 pyramids are ca. 5 times higher than that of pure DNA scaffolds with a little blue shift (Figure S10), which was attributed to the coupling effect of plasmonic NPs in the hybrid structures. The characteristics of chiral interactions in hybrid molecular-metal structures are very different from purely molecular systems.

Especially, the CD signal of DNA would change a lot when CD of the NPs at visible range was very strong which is in agreement with previous reports.[13,21]

CONCLUSIONS

We have demonstrated the successful preparation of hetero-particle chiral pyramids using a DNA-driven self-assembly process and investigated their chiroptical properties. Applic-ability of the described assembly technique to different kinds of metal and/or semiconductor NPs instills confidence that the position of CD signals can be varied in a wide range of UV and visible wavelengths, 350−550 nm, with a strong potential to be extended into the near-IR region for narrow-bandgap quantum dots. High yields of pyramid preparation and the possibility of its scalable synthesis using automated polymerase chain reaction should promote the development of chiral materials in biological applications as well as negative refractive index materials.

ASSOCIATED CONTENT

Ⓢ Supporting Information

Materials and detailed experimental procedures; supplementary table and figures. This material is available free of charge via the Internet at http://pubs.acs.org.

AUTHOR INFORMATION

Corresponding Author
khecho@163.com; wanglb1@126.com; kotov@umich.edu
Author Contributions
#W.Y., L.X., C.X., and W.M. contributed equally.
Notes
The authors declare no competing financial interest.

ACKNOWLEDGMENTS

1036672) that were used to maintain equipment used in this study.

■ REFERENCES

(1) Wagnière, G. H. *On chirality and the universal asymmetry: reflections on image and mirror image*; Wiley-VCH: Weinheim, Germany, 2007.

(2) Noguez, C.; Garzon, I. L. *Chem. Soc. Rev.* **2009**, *38*, 757−771.

(3) Zhou, Y. L.; Yang, M.; Sun, K.; Tang, Z. Y.; Kotov, N. A. *J. Am. Chem. Soc.* **2010**, *132*, 6006−6013.

(4) Govorov, A. O.; Gun'ko, Y. K.; Slocik, J. M.; Gerard, V. A.; Fan, Z. Y.; Naik, R. R. *J. Mater. Chem.* **2011**, *21*, 16806−16818.

(5) Gautier, C.; Burgi, T. *ChemPhysChem* **2009**, *10*, 483−492.

(6) Nakashima, T.; Kobayashi, Y.; Kawai, T. *J. Am. Chem. Soc.* **2009**, *131*, 10342−10343.

(7) Elliott, S. D.; Moloney, M. P.; Gun'ko, Y. K. *Nano Lett.* **2008**, *8*, 2452−2457.

(8) Li, Y. Y.; Zhou, Y. L.; Wang, H. Y.; Perrett, S.; Zhao, Y. L.; Tang, Z. Y.; Nie, G. J. *Angew. Chem., Int. Ed.* **2011**, *50*, 5860−5864.

(9) Govan, J. E.; Jan, E.; Querejeta, A.; Kotov, N. A.; Gun'ko, Y. K. *Chem. Commun.* **2010**, *46*, 6072−6074.

(10) Guerrero-Martinez, A.; Auguie, B.; Alonso-Gomez, J. L.; Dzolic, Z.; Gomez-Grana, S.; Zinic, M.; Cid, M. M.; Liz-Marzan, L. M. *Angew. Chem., Int. Ed.* **2011**, *50*, 5499−5503.

(11) Lieberman, I.; Shemer, G.; Fried, T.; Kosower, E. M.; Markovich, G. *Angew. Chem., Int. Ed.* **2008**, *47*, 4855−4857.

(12) Oh, H. S.; Liu, S.; Jee, H.; Baev, A.; Swihart, M. T.; Prasad, P. N. *J. Am. Chem. Soc.* **2010**, *132*, 17346−17348.

(13) Petty, J. T.; Zheng, J.; Hud, N. V.; Dickson, R. M. *J. Am. Chem. Soc.* **2004**, *126*, 5207−5212.

(14) Shemer, G.; Krichevski, O.; Markovich, G.; Molotsky, T.; Lubitz, I.; Kotlyar, A. B. *J. Am. Chem. Soc.* **2006**, *128*, 11006−11007.

(15) Naik, R. R.; Slocik, J. M.; Govorov, A. O. *Nano Lett.* **2011**, *11*, 701−705.

(16) Sánchez-Castillo, A.; Román-Velázquez, C.; Noguez, C. *Phys. Rev. B* **2006**, *73*, 045401.

(17) George, J.; Thomas, K. G. *J. Am. Chem. Soc.* **2010**, *132*, 2502−2503.

(18) Auguie, B.; Alonso-Gomez, J. L.; Guerrero-Martinez, A.; Liz-Marzan, L. M. *J. Phys. Chem. Lett.* **2011**, *2*, 846−851.

(19) Guo, X. M.; Jiang, C.; Shi, T. S. *Inorg. Chem.* **2007**, *46*, 4766−4768.

(20) Dolamic, I.; Knoppe, S.; Dass, A.; Bürgi, T. *Nat. Commun.* **2012**, *3*, 798.

(21) Chen, W.; Bian, A.; Agarwal, A.; Liu, L. Q.; Shen, H. B.; Wang, L. B.; Xu, C. L.; Kotov, N. A. *Nano Lett.* **2009**, *9*, 2153−2159.

(22) Mastroianni, A. J.; Claridge, S. A.; Alivisatos, A. P. *J. Am. Chem. Soc.* **2009**, *131*, 8455−8459.

(23) (a) Srivastava, S.; Santos, A.; Critchley, K.; Kim, K.-S.; Podsiadlo, P.; Sun, K.; Lee, J.; Xu, C.; Lilly, G. D.; Glotzer, S. C.; Kotov, N. A. *Science* **2010**, *327*, 1355−1359. (b) Lilly, G. D.; Agarwal, A.; Srivastava, S.; Kotov, N. A. *Small* **2011**, *7*, 2004−2009.

(24) Kuzyk, A.; Schreiber, R.; Fan, Z. Y.; Pardatscher, G.; Roller, E. M.; Hogele, A.; Simmel, F. C.; Govorov, A. O.; Liedl, T. *Nature* **2012**, *483*, 311−314.

(25) Shen, X. B.; Song, C.; Wang, J. Y.; Shi, D. W.; Wang, Z. A.; Liu, N.; Ding, B. Q. *J. Am. Chem. Soc.* **2012**, *134*, 146−149.

(26) Hentschel, M.; Schaferling, M.; Weiss, T.; Liu, N.; Giessen, H. *Nano Lett.* **2012**, *12*, 2542−2547.

(27) Pendry, J. *Science* **2004**, *306*, 1353−1355.

(28) Decker, M.; Klein, M.; Wegener, M.; Linden, S. *Opt. Lett.* **2007**, *32*, 856−858.

(29) Li, Z.; Zhu, Z.; Liu, W.; Zhou, Y.; Han, B.; Gao, Y.; Tang, Z. *J. Am. Chem. Soc.* **2012**, *134*, 3322−3325.

(30) Mirkin, C. A.; L., R. L.; Mucic, R. C.; Storhoff, J. J. *Nature* **1996**, *382*, 607−609.

(31) Alivisatos, A. P.; Johnsson, K. P.; Peng, X.; Wilson, T. E.; Loweth, C. J.; Bruchez, M. P.; Schultz, P. G. *Nature* **1996**, *382*, 609−611.

(32) Wang, L.; Xu, L.; Kuang, H.; Xu, C.; Kotov, N. A. *Acc. Chem. Res.* **2012**, DOI: 10.1021/ar200305f.

(33) Fan, Z. Y.; Govorov, A. O. *Nano Lett.* **2010**, *10*, 2580−2587.

(34) Zhao, Y.; Xu, L.; Kuang, H.; Wang, L.; Xu, C. *J. Mater. Chem.* **2012**, *22*, 5574−5580.

(35) Frens, G. *Nature* **1973**, *241*, 20−22.

(36) Slot, J. W.; Geuze, H. J. *Eur. J. Cell. Biol.* **1985**, *38*, 87−93.

(37) Loweth, C. J.; Caldwell, W. B.; Peng, X.; Alivisatos, A. P.; Schultz, P. G. *Angew. Chem., Int. Ed.* **1999**, *38*, 1808−1812.

(38) Sun, Y.; Xia, Y. *Adv. Mater.* **2003**, *15*, 695−699.

(39) Liu, L.; Wei, T.; Guan, X.; Zi, X.; He, H.; Dai, H. *J. Phys. Chem. C* **2009**, *113*, 8595−8600.

(40) Zanchet, D.; Micheel, C. M.; Parak, W. J.; Gerion, D.; Alivisatos, A. P. *Nano Lett.* **2001**, *1*, 32−35.

(41) Chen, G.; Wang, Y.; Tan, L. H.; Yang, M. X.; Tan, L. S.; Chen, Y.; Chen, H. Y. *J. Am. Chem. Soc.* **2009**, *131*, 4218−4219.

(42) Chen, W.; Xu, D. H.; Liu, L. Q.; Peng, C. F.; Zhu, Y. Y.; Ma, W.; Bian, A.; Li, Z.; Yuanyuan; Jin, Z. Y.; Zhu, S. F.; Xu, C. L.; Wang, L. B. *Anal. Chem.* **2009**, *81*, 9194−9198.

(43) Bakalova, R.; Zhelev, Z.; Ohba, H.; Baba, Y. *J. Am. Chem. Soc.* **2005**, *127*, 11328−11335.

(44) Wang, Q.; Wang, H.; Lin, C.; Sharma, J.; Zou, S.; Liu, Y. *Chem. Commun.* **2009**, *46*, 240−242.

(45) Xiao, Y.; Pavlov, V.; Gill, R.; Bourenko, T.; Willner, I. *ChemBioChem* **2004**, *5*, 374−379.

(46) Claridge, S. A.; Goh, S. L.; Frechet, J. M. J.; Williams, S. C.; Micheel, C. M.; Alivisatos, A. P. *Chem. Mater.* **2005**, *17*, 1628−1635.

(47) Tokareva, I.; Hutter, E. *J. Am. Chem. Soc.* **2004**, *126*, 15784−15789.

(48) Crick, F. *Nature* **1974**, *248*, 766−769.

(49) Macfarlane, R. J.; Lee, B.; Hill, H. D.; Senesi, A. J.; Seifert, S.; Mirkin, C. A. *Proc. Natl. Acad. Sci. U.S.A.* **2009**, *106*, 10493−10498.

(50) Nykypanchuk, D.; Maye, M. M.; van der Lelie, D.; Gang, O. *Nature* **2008**, *451*, 549−552.

(51) Xu, L. G.; Kuang, H.; Xu, C. L.; Ma, W.; Wang, L. B.; Kotov, N. A. *J. Am. Chem. Soc.* **2012**, *134*, 1699−1709.

(52) Park, S. Y.; Lytton-Jean, A. K. R.; Lee, B.; Weigand, S.; Schatz, G. C.; Mirkin, C. A. *Nature* **2008**, *451*, 553−556.

(53) Buda, A. B.; Mislow, K. *J. Am. Chem. Soc.* **1992**, *114*, 6006−6012.

(54) Kosower, E. M.; de Souza, J. R. *Chem. Phys.* **2006**, *324*, 3−7.

(55) Berova, N.; Di Bari, L.; Pescitelli, G. *Chem. Soc. Rev.* **2007**, *36*, 914−931.

(56) Guerrero-Martínez, A.; Alonso-Gómez, J. L.; Auguié, B.; Cid, M. M.; Liz-Marzán, L. M. *Nano Today* **2011**, *6*, 381−400.

(57) Roman-Velazquez, C. E.; Noguez, C. *J. Chem. Phys.* **2011**, *134*, 4116.

(58) Govorov, A. O.; Fan, Z. Y.; Hernandez, P.; Slocik, J. M.; Naik, R. R. *Nano Lett.* **2010**, *10*, 1374−1382.